Solution for Laminar Compressible Axisymmetric Jets Issuing into Stagnant and Moving Mediums

N.A. Ghazzawi, N.J. Rabadi and B.B. Hijazen
Mech. Eng. Dept., Eng. & Tech. Fac.,
University of Jordan, Amman, Jordan

Abstract. A numerical study is conducted for laminar compressible axisymmetric jets. The outer medium into which the jet is injected is considered to be at rest or moving parallel to the jet. Two values of the outer medium velocity are investigated while four types of the injected gas are considered, namely carbon dioxide, oxygen, ammonia and hydrogen. An implicit finite difference method is used to solve the boundary layer equations governing the jet flow. A coordinate transformation is used to improve the efficiency and accuracy of the numerical scheme. Results for the velocity profiles and mixture fraction profiles are obtained. An analysis of these results is made and a criterion for comparing the velocity and mixture fraction decay rates for the considered gases is established.

1. Introduction

A considerable amount of work[1-5] has been done on jets because of their importance in a wide variety of engineering applications. Some of these applications are: Jet flow inside combustion chambers, jets in aerospace devices, jet pumps and ejectors, discharge of effluents and discharges from draft tubes and certain outlets into rivers.

A subsonic jet discharging from a tube can always be considered as fully expanded. For a jet cross section to remain round and the trajectory to remain straight, it is necessary that there would be no force acting on the jet in the lateral direction. This also requires that the medium into which the jet is discharged be at rest or flowing in the same direction, and the body forces are negligible.

If a primary jet of gas issues into a secondary stream which is composed of a different gas, diffusion becomes one of the most important mechanisms in the mixing process. The diffusion equation must then be included in the basic equations along with the proper equation of state, and the properties must be evaluated using the methods required for gas mixtures.

Pai[6] discussed the jet mixing of different gases, and the basic equations for diffusion are found in Rohensow *et al.*[7] and Bird *et al.*[8]. Hornbeck[9] put forward the finite difference representation for the plate mixing of jets but didn't check his suggested scheme.

The prediction of free shear flows was for a long time most commonly done by integral methods, but now the differential methods have become the center of interest for most researchers[9].

In the present work, the formulation for the mixing of an asixymmetric jet of gas with a moving or stationary stream of air at the same temperature is considered. The gases considered are those of carbon dioxide, oxygen, ammonia and hydrogen. An implicit finite difference method is used to solve the boundary layer equations governing the jet flow and a coordinate transformation is used to improve the efficiency and accuracy of the numerical scheme. An analysis of the obtained results shows that they are sensitive to the selection of the initial conditions at the nozzle exit.

2. Analysis

Figure 1 shows a schematic diagram for a jet of diameter $2a$ issuing into the ambient. The Reynolds number is large enough so that the boundary layer approximation can be invoked. The general assumptions made in formulating the governing equations are

1. Axisymmetric flow, (circular or round jet).
2. Uniform pressure.
3. No swirl.
4. All properties are constant except the density.
5. Mass transfer due to diffusion involves a negligible momentum flux.
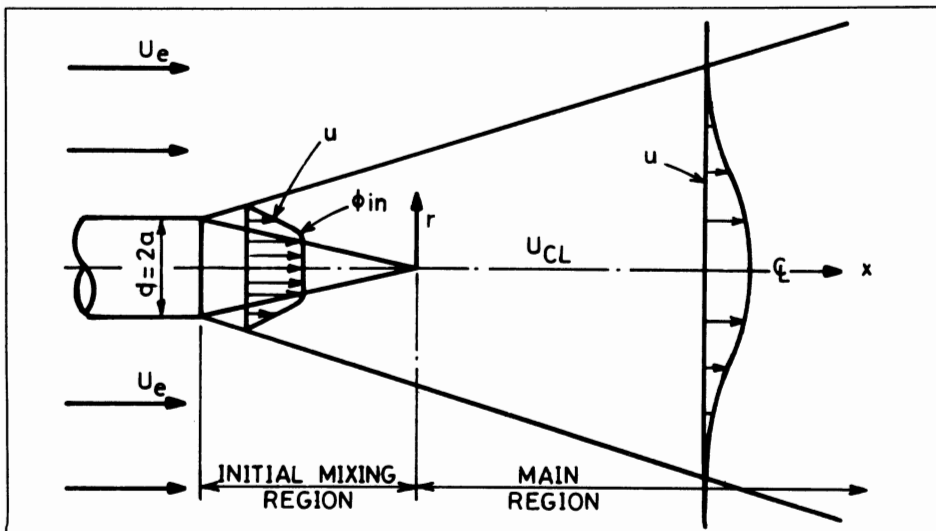

FIG. 1. Schematic diagram for an axisymmetric jet issuing into an ambient.

With these assumptions, the governing equations for the conservation of momentum, concentration and mass are as follows:

momentum

$$\rho(u\frac{\partial u}{\partial x}+\upsilon\frac{\partial u}{\partial r})=\frac{\mu}{r}\frac{\partial}{\partial r}(r\frac{\partial u}{\partial r}) \tag{1}$$

mass diffusion

$$\rho(u\frac{\partial f}{\partial x}+\upsilon\frac{\partial f}{\partial r})=\frac{D}{r}\frac{\partial}{\partial r}(r\rho\frac{\partial f}{\partial r}) \tag{2}$$

and, continuity

$$\frac{\partial(\rho u)}{\partial x}+\frac{1}{r}\frac{\partial(\rho r\upsilon)}{\partial r}=0 \tag{3}$$

where u is the axial velocity, υ is the lateral velocity, f is the mixture fraction given by the ratio of the weight of the discharged gas to that of the mixture, ρ is the density, μ is the viscosity, D is the diffusion coefficient, τ is the radial coordinate and x is the axial coordinate.

The initial conditions ($x = 0$) can be taken as uniform profiles except for u, where it is more reasonable to assume a parabolic profile at the nozzle exit. Mathematically, these conditions are

$$u = u_{in}(1-(\frac{r}{a})^2), \qquad f = 1.0, \quad \text{at} \quad r \leq a \tag{4}$$

$$u = u_e, \qquad\qquad\qquad f = 0.0, \quad \text{at} \quad r > a$$

The boundary conditions for axisymmetric jet flows are

$$\frac{\partial u}{\partial r} = \frac{\partial f}{\partial r} = \upsilon = 0.0 \qquad \text{at} \quad r = 0.0 \tag{5}$$

$$u = u_e, f = 0.0 \qquad \text{at} \quad r \to \infty$$

The governing equations may be put in dimensionless form by the following choice of dimensionless variables

$$U = \frac{u}{u_{in}}, \mu^* = \frac{\mu}{\mu_0}, \rho^* = \frac{\rho}{\rho_0} \tag{6}$$

$$V = \frac{\rho_0 \upsilon a}{\mu_0}, R = \frac{r}{a}, X = \frac{x\mu_0}{\rho_0 u_{in} a^2} = \frac{x}{aRe}$$

where $Re = \rho_0 u_{in} a/\mu_0$

For these dimensionless representations, the conditions of air at standard atmospheric conditions (1 atm, 298 K) have been chosen for reference values. The concentration f is already dimensionless. Inserting these variables into Equations (1) to (3) gives

$$\rho^*(U\frac{\partial U}{\partial X}+V\frac{\partial U}{\partial R})=\frac{\mu^*}{R}\frac{\partial}{\partial R}(R\frac{\partial U}{\partial R}) \tag{7}$$

$$\rho^*(U\frac{\partial f}{\partial X}+V\frac{\partial f}{\partial R})=\frac{\Pi}{R}\frac{\partial}{\partial R}(\rho^*R\frac{\partial f}{\partial R}) \tag{8}$$

$$\frac{\partial(\rho^* U)}{\partial X} + \frac{1}{R}\frac{\partial}{\partial R}(\rho^* RV) = 0 \tag{9}$$

where $\Pi = \mu^* RMC/Sc$, $Sc = \mu/\rho D$ and $RMC = \rho_0/\rho_j$ = ratio of the density of the surrounding air at the reference conditions to that of the jet at the nozzle exit.

The normalized initial conditions are

$$U = 1 - R^2, f = 1.0 \quad \text{at} \quad R \le 1 \tag{10}$$

$$U = CO, f = 0.0 \text{ at} \quad R > 1$$

where

$$CO = u_e/u_{in}$$

The normalized boundary conditions are

$$\frac{\partial U}{\partial R} = \frac{\partial f}{\partial R} = V = 0.0 \quad \text{at} \quad R = 0.0 \tag{11}$$

$$U = CO, f = 0.0 \quad \text{at} \quad R \to \infty$$

An equation of state for the gas mixture is now required in order to express ρ as a function of f, ρ_0 and ρ_j. The derivation of this equation is straightforward and only the final result will be given here[*].

$$\rho^* = \frac{1}{1 + (RMC - 1)f} \tag{12}$$

Therefore, Equations (7), (8), (9) and (12) are solved for U, f, V and ρ^*, respectively. The jets considered are those of carbon dioxide, oxygen, ammonia and hydrogen. The values of CO considered are 0.0, 0.5 and 0.75. The values of μ^*, RMC and Sc number for these cases are obtained from Ref. [10]. These values are shown in Table 1.

TABLE 1. Values of RMC, μ^* and Sc for the tested cases.

Type of jet	RMC	μ^*	Sc
Carbon dioxide into air	0.655	0.810	0.94
Oxygen into air	0.90	1.117	0.75
Ammonia into air	1.694	0.556	0.78
Hydrogen into air	14.4	0.486	0.22

3. Method of Solution

To make the numerical calculations more efficient, two transformations are employed in the present study.

3.1 Numerical Solution in (R – X) Coordinates (First Transformation)

The numerical solution for Equations (7), (8) and (9) is obtained by choosing a finite difference representation for these equations. The finite difference grid is shown in Fig. (2). The difference form selected for these equations is highly implicit in that, not only

---

[*]See Ref. [10] for more details.

are all R derivatives evaluated at $j + 1$ but also, the coefficients of the nonlinear convective terms are evaluated at $j + 1$. This representation is necessary if zero and small freestream velocities are to be considered, since the usual implicit scheme with the coefficients evaluated at j is inconsistent for these conditions. For zero freestream velocity the usual implicit form results in the U velocity profile decreasing linearly from the edge of the jet to whatever value of R is chosen as infinity. This result is obviously incorrect.
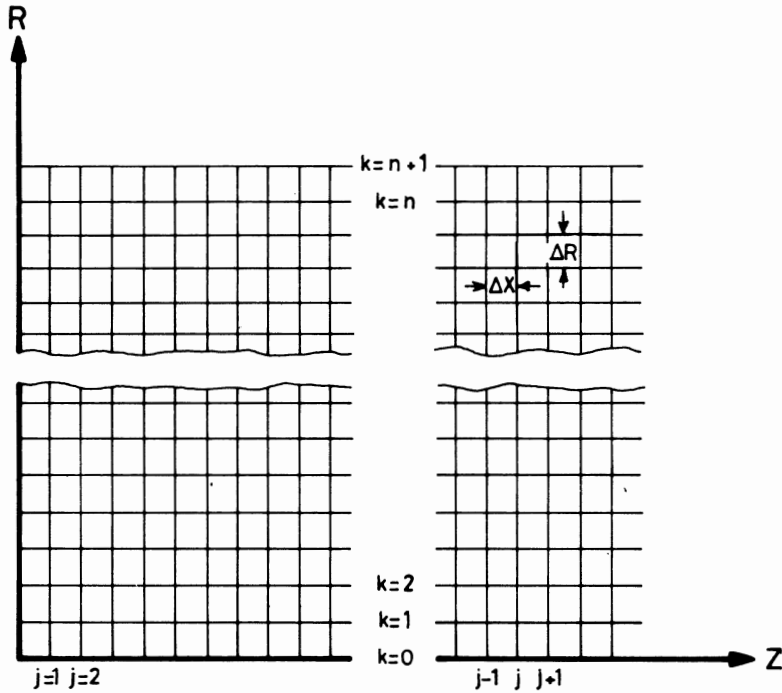
FIG. 2. Finite difference grid for axisymmetric jet.

The nonlinear difference representation chosen here is valid for all values of CO. The representation of the momentum equation (7)

$$\rho_{j+1,k}^{*(l)} \, [U_{j+1,k}^{(l)} \, \frac{U_{j+1,k}^{(l+1)} - U_{j,k}}{\Delta X} + V_{j+1,k}^{(l)} \, \frac{U_{j+1,k+1}^{(l+1)} - U_{j+1,k-1}^{(l+1)}}{2(\Delta R)}] \tag{13}$$

$$= \mu^* \{ \frac{1}{R_k} \, \frac{U_{j+1,k+1}^{(l+1)} - U_{j+1,k-1}^{(l+1)}}{2(\Delta R)} + \frac{U_{j+1,k+1}^{(l+1)} - 2U_{j+1,k}^{(l+1)} + U_{j+1,k-1}^{(l+1)}}{(\Delta R)^2} \}$$

where the superscripts are used to indicate on which iteration that value was obtained; for example $U_{j+1,k}^{(l)}$ is obtained on the (l)th iteration while $U_{j+1,k}^{(l+1)}$ is obtained on the $(l+1)$ th iteration.

It is useful to rewrite Equation (13) as

$$\alpha_k^{(l)} U_{j+1,k-1}^{(l+1)} + \beta_k^{(l)} U_{j+1,k}^{(l+1)} + \Omega_k^{(l)} U_{j+1,k+1}^{(l+1)} = \Phi_k^{(l)} \tag{14}$$

where

$$\alpha_k^{(l)} = \frac{-\rho_{j+1,k}^{*(l)} V_{j+1,k}^{(l)}}{2(\Delta R)} - \frac{\mu^*}{(\Delta R)^2} + \frac{\mu^*}{2(R_k)\Delta R} \tag{15}$$

$$\beta_k^{(l)} = \frac{\rho_{j+1,k}^{*(l)} U_{j+1,k}^{(l)}}{\Delta X} + \frac{2\mu^*}{(\Delta R)^2} \tag{16}$$

$$\Omega_k^{(l)} = \frac{\rho_{j+1,k}^{*(l)} V_{j+1,k}^{(l)}}{2(\Delta R)} - \frac{\mu^*}{(\Delta R)^2} - \frac{\mu^*}{2(R_k)\Delta R} \tag{17}$$

$$\Phi_k^{(l)} = \frac{\rho_{j+1,k}^{*(l)} U_{j+1,k}^{(l)} U_{j,k}}{\Delta X} \tag{18}$$

The value of $\alpha_k^{(l)}$ and $\Omega_k^{(l)}$ at $k = 0$ (the centerline) are infinite. To overcome this problem, the limit of momentum equation (7) is taken as $\eta \to 0$. Doing this, and discretizing the resulting equation in the same manner used above, the coefficients at $k = 0$ can be calculated as

$$\alpha_0^{'(l)} = 0.0 \tag{19}$$

$$\beta_0^{(l)} = \frac{\rho_{j+1,0}^{*(l)} U_{j+1,0}^{(l)}}{\Delta X} + \frac{4\mu^*}{(\Delta R)^2} \tag{20}$$

$$\Omega_0^{(l)} = \frac{-4\mu^*}{(\Delta R)^2} \tag{21}$$

$$\Phi_0^{(l)} = \frac{\rho_{j+1,0}^{*(l)} U_{j+1,0}^{(l)} U_{j,0}}{\Delta X} \tag{22}$$

The continuity equation can be discretized in the same manner to get

$$V_{j+1,k+1}^{(l+1)} = \frac{\rho_{j+1,k}^{*(l)} R_k}{\rho_{j+1,k+1}^{*(l)} R_{k+1}} V_{j+1,k}^{(l+1)} + \frac{R_k \Delta R}{R_{k+1} \Delta X} \frac{\rho_{j,k}^* U_{j,k} - \rho_{j+1,k}^{*(l+1)} U_{j+1,k}^{(l+1)}}{\rho_{j+1,k+1}^{*(l)}} \tag{23}$$

This equation is valid for $k > 0$. The continuity equation at $k = 0$ is

$$V_{j+1,1}^{(l+1)} = \frac{\Delta R}{2(\Delta X)} \left[\frac{\rho_{j,0}^*}{\rho_{j+1,0}^{*(l)}} U_{j,0} - U_{j+1,k}^{(l+1)} \right] \tag{24}$$

Thus all values of $V_{j+1,k+1}^{(l)}$ can be found in a stepwise manner by working outward from the centerline of the jet.

Also, the discretized form of the mass diffusion equation may be written as

$$\alpha_k^{'(l)} f_{j+1,k-1}^{(l+1)} + \beta_k^{'(l)} f_{j+1,k}^{(l+1)} + \Omega_k^{'} f_{j+1,k+1}^{(l+1)} = \Phi_k^{'(l)} \tag{25}$$

where

$$\alpha_k^{\prime(l)} = \frac{-\rho_{j+1,k}^{*(l)} V_{j+1,k}^{(l)}}{2(\Delta R)} - \frac{\Pi \rho_{j+1,k}^{*(l)}}{(\Delta R)^2} + \frac{\Pi \rho_{j+1,k}^{*(l)}}{2(R_k)(\Delta R)} + \Pi \frac{\rho_{j+1,k+1}^{*(l)} - \rho_{j+1,k-1}^{*(l)}}{4(\Delta R)^2} \tag{26}$$

$$\beta_k^{\prime(l)} = \frac{\rho_{j+1,k}^{*(l)} U_{j+1,k}^{(l)}}{\Delta X} + \frac{2\Pi \rho_{j+1,k}^{*(l)}}{(\Delta R)^2} \tag{27}$$

$$\Omega_k^{\prime(l)} = \frac{\rho_{j+1,k}^{*(l)} V_{j+1,k}^{(l)}}{2(\Delta R)} - \frac{\Pi \rho_{j+1,k}^{*(l)}}{(\Delta R)^2} - \frac{\Pi \rho_{j+1,k}^{*(l)}}{2(R_k(\Delta R)} - \frac{\Pi(\rho_{j+1,k+1}^{*(l)} - \rho_{j+1,k-1}^{*(l)})}{4(\Delta R)^2} \tag{28}$$

$$\Phi_k^{\prime(l)} = \frac{\rho_{j+1,k}^{*(l)} U_{j+1,k}^{(l)} f_{j,k}}{\Delta X} \tag{29}$$

The value of $\alpha_k^{\prime(l)}$ and $\Omega_k^{\prime(l)}$ at $k = 0$ (the centerline) can be found by taking the limit of the mass equation (8) as $\eta \to 0$. This results in

$$\alpha_0^{\prime(l)} = 0.0 \tag{30}$$

$$\beta_0^{\prime(l)} = \frac{\rho_{j+1,0}^{*(l)} U_{j+1,0}^{(l)}}{\Delta X} + \frac{4\Pi \rho_{j+1,k}^{*(l)}}{(\Delta R)^2} \tag{31}$$

$$\Omega_0^{\prime(l)} = \frac{-4\Pi \rho_{j+1,k}^{*(l)}}{(\Delta R)^2} \tag{32}$$

$$\Phi_0^{\prime(l)} = \frac{\rho_{j+1,0}^{*(l)} U_{j+1,0}^{(l)} U_{j,0}}{\Delta X} \tag{33}$$

Also, the finite difference form of the equation of state is

$$\rho_{j+1,k}^{*(l+1)} = \frac{1}{1 + (RMC - 1) f_{j+1,k}^{(l+1)}} \tag{34}$$

The solution starts by guessing values for the unknown velocity and mixture fraction profiles. These are usually taken at the preceding step upstream. Substituting these guessed values into Equation (14), a new velocity profile can be calculated. Using Equation (23), a new lateral velocity profile can be obtained. Also, a new mixture fraction profile can be obtained from Equation (25). The density can then be calculated from Equation (34). These calculated profiles are used, after applying underrelaxation, as a new guess and the iteration process continues until convergence. When convergence is attained, another step downstream is moved. A flow chart that illustrates this method of solution is shown in Fig. (3). Of special interest is to note that the sets of equations resulting from Equations (14) and (25) are tridiagonal sets and may be solved easily using any tridiagonal solver while Equation (23) gives an explicit relation for the lateral velocity so that it can be calculated directly by working outward from the center of the jet.

The values of step sizes used in the solution are $\Delta R = 0.05$ and $\Delta X = 0.001$. The accuracy of the obtained results has been checked by running the computer code for

(1)ΔR = 0.025 and ΔX = 0.0005 and (2)ΔR = 0.1 and ΔX = 0.002. The results in both cases were comparable with the original results at least up to three significant figures.
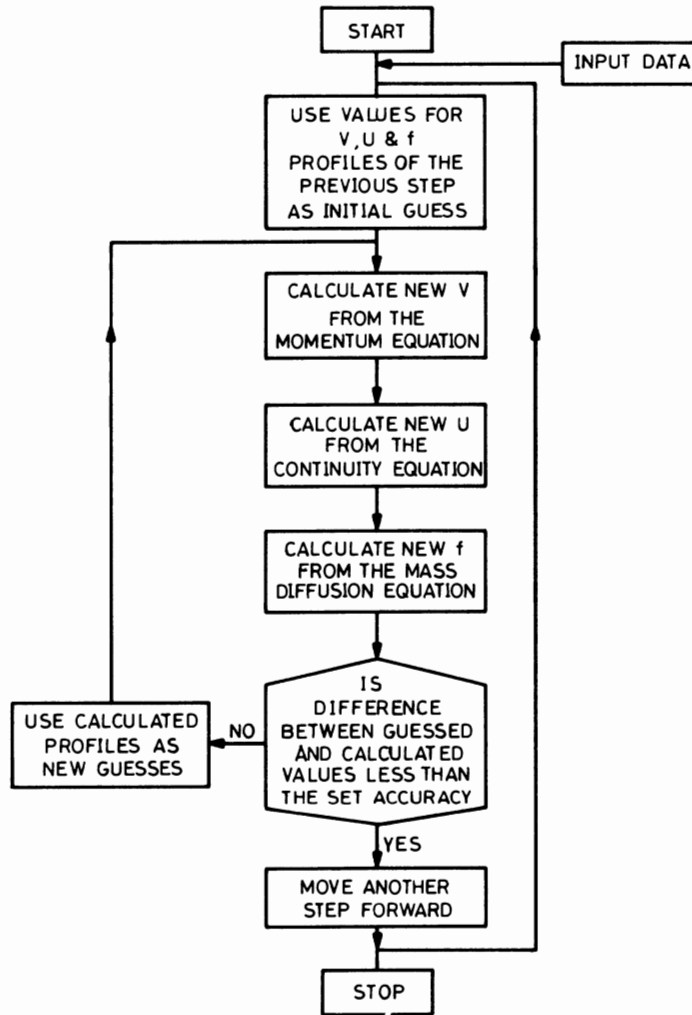

FIG. 3. Flow chart showing the method of solution.

3.2 Numerical Solution in the ($\eta - \zeta$) Coordinates (Second Transformation)

In order to remove the jet growths, Kee and Miller[11] used the following transformation

$$\eta(r,x) = \frac{r}{x}, \zeta(x) = x \tag{35}$$

In the present study, η and ζ are defined by

$$\eta(R, X) = \frac{R}{X}, \zeta(X) = X \tag{36}$$

Using the chain rule, the governing equations in the $(\eta - \zeta)$ plane can be obtained as:

momentum

$$\rho^* U \zeta \frac{\partial U}{\partial \zeta} + \frac{V_1}{\eta} \frac{\partial U}{\partial \eta} = \frac{\mu^*}{\eta \zeta} \frac{\partial}{\partial \eta} (\eta \frac{\partial U}{\partial \eta}) \tag{37}$$

mass diffusion,

$$\rho^* U \zeta \frac{\partial f}{\partial \zeta} + \frac{V_1}{\eta} \frac{\partial f}{\partial \eta} = \frac{\Pi}{\eta \zeta} \frac{\partial}{\partial \eta} (\eta \rho^* \frac{\partial f}{\partial \eta}) \tag{38}$$

and, continuity

$$\zeta \frac{\partial \rho^* U}{\partial \zeta} + \frac{1}{\eta} \frac{\partial V_1}{\eta} + 2\rho^* U = 0 \tag{39}$$

where

$$V_1 = \eta \rho^* V - \eta^2 \rho^* U \tag{40}$$

and the boundary conditions become

$$\frac{\partial U}{\partial \eta} |_{\eta=0} = \frac{\partial f}{\partial \eta} |_{\eta=0} = V(0, \zeta) = 0 \tag{41}$$

$$U(\eta, \zeta) = CO \quad \text{at} \quad \eta \to \infty$$

The momentum and the mass diffusion equations (37) and (38) can be expanded as

$$\rho^* U \zeta \frac{\partial U}{\partial \zeta} + (\frac{V_1}{\eta} - \frac{\mu^*}{\eta \zeta}) \frac{\partial U}{\partial \eta} = \frac{\mu^*}{\zeta} \frac{\partial^2 U}{\partial \eta^2} \tag{42}$$

$$\rho^* U \zeta \frac{\partial f}{\partial \zeta} + (\frac{V_1}{\eta} - \frac{\Pi \rho^*}{\eta \zeta}) \frac{\partial f}{\partial \eta} = \frac{\Pi \rho^*}{\zeta} \frac{\partial^2 f}{\partial \eta^2} + \frac{\Pi}{\zeta} \frac{\partial f}{\partial \eta} \frac{\partial \rho^*}{\partial \eta} \tag{43}$$

The governing equations (42), (43) and (39) may be finite differenced in the same way used for the first transformation. Only the results will be given here. The momentum equation (42) may be written as

$$A1_k^{(l)} U_{j+1,k-1}^{(l+1)} + B1_k^{(l)} U_{j+1,k}^{(l+1)} + C1_k^{(l)} U_{j+1,k+1} = D1_k^{(l)} \tag{44}$$

where

$$A1_k^{(l)} = -\frac{V_{1_{j+1,k}}^{(l)}}{2\eta_k \Delta \eta} + \frac{\mu^*}{2\eta_k \zeta_{j+1} \Delta \eta} - \frac{\mu^*}{\zeta_{j+1} (\Delta \eta)^2} \tag{45}$$

$$B1_k^{(l)} = \frac{\rho_{j+1,k}^{*(l)} U_{j+1,k}^{(l)} \zeta_{j+1}}{\Delta \zeta} + \frac{2\mu^*}{\zeta_{j+1} (\Delta \eta)^2} \tag{46}$$

$$C1_k^{(l)} = \frac{V_{1_{j+1,k}}^{(l)}}{2\eta_k \Delta \eta} - \frac{\mu^*}{2\eta_k \zeta_{j+1} \Delta \eta} - \frac{\mu^*}{\zeta_{j+1} (\Delta \eta)^2} \tag{47}$$

$$D1_k^{(l)} = \frac{\rho_{j+1,k}^{*(l)} U_{j,k} U_{j+1,k}^{(l)} \zeta_{j+1}}{\Delta \zeta} \tag{48}$$

At $k = 0$, the coefficients are obtained by taking the limit of Equation (42) as $\eta \to 0$. The result is

$$A1_0^{(l)} = 0.0 \tag{49}$$

$$B1_0^{(l)} = \frac{\zeta_{j+1}\,\rho_{j+1,0}^{*(l)}\,U_{j+1,0}^{(l)}}{\Delta\zeta} + \frac{4\mu^*}{\zeta_{j+1}(\Delta\eta)^2} \tag{50}$$

$$C1_0^{(l)} = \frac{-4\mu^*}{\zeta_{j+1}(\Delta\eta)^2} \tag{51}$$

$$D1_0^{(l)} = \frac{\zeta_{j+1}\,\rho_{j+1,0}^{*(l)}\,U_{j,0}\,U_{j+1,0}^{(l)}}{\Delta\zeta} \tag{52}$$

Also, the mass diffusion equation (43) may be written as

$$A2_k^{(l)}\,f_{j+1,k-1}^{(l+1)} + B2_k^{(l)}\,f_{j+1,k}^{(l+1)} + C2_k^{(l)}\,f_{j+1,k+1} = D2_k^{(l)} \tag{53}$$

where

$$A2_k^{(l)} = -\frac{V_{1_{j+1,k}}^{(l)}}{2\eta_k\Delta\eta} + \frac{\Pi\rho_{j+1,k}^{*(l)}}{2\eta_k\zeta_{j+1}\Delta\eta} - \frac{\Pi\rho_{j+1,k}^{*(l)}}{\zeta_{j+1}(\Delta\eta)^2} + \frac{\Pi}{\zeta_{j+1}}\frac{\rho_{j+1,k+1}^{*(l)} - \rho_{j+1,k-1}^{*(l)}}{4(\Delta\eta)^2} \tag{54}$$

$$B2_k^{(l)} = \frac{\rho_{j+1,k}^{*(l)}U_{j+1,k}^{(l)}\zeta_{j+1}}{\Delta\zeta} + \frac{2\Pi\rho_{j+1,k}^{*(l)}}{\zeta_{j+1}(\Delta\eta)^2} \tag{55}$$

$$C2_k^{(l)} = \frac{V_{1_{j+1,k}}^{(l)}}{2\eta_k\Delta\eta} - \frac{\Pi\rho_{j+1,k}^{*(l)}}{2\eta_k\zeta_{j+1}\Delta\eta} - \frac{\Pi\rho_{j+1,k}^{*(l)}}{\zeta_{j+1}(\Delta\eta)^2} - \frac{\Pi}{\zeta_{j+1}}\frac{\rho_{j+1,k+1}^{*(l)} - \rho_{j+1,k-1}^{*(l)}}{4(\Delta\eta)^2} \tag{56}$$

$$D2_k^{(l)} = \frac{\rho_{j+1,k}^{*(l)}f_{j,k}U_{j+1,k}^{(l)}\zeta_{j+1}}{\Delta\zeta} \tag{57}$$

At $k = 0$, the coefficients are obtained by taking the limit of Equation (43) as $\eta \to 0$. The result is

$$A2_0^{(l)} = 0.0 \tag{58}$$

$$B2_0^{(l)} = \frac{\zeta_{j+1}\rho_{j+1,0}^{*(l)}U_{j+1,0}^{(l)}}{\Delta\zeta} + \frac{4\Pi\rho_{j+1,0}^{*(l)}}{\zeta_{j+1}(\Delta\eta)^2} \tag{59}$$

$$C2_0^{(l)} = \frac{-4\Pi\rho_{j+1,0}^{*(l)}}{\zeta_{j+1}(\Delta\eta)^2} \tag{60}$$

$$D2_0^{(l)} = \frac{\zeta_{j+1}\rho_{j+1,0}^{*(l)}f_{j,0}U_{j+1,0}^{(l)}}{\Delta\zeta} \tag{61}$$

and the finite difference form of the continuity equation (39) is

$$V_{1_{j+1,k+1}}^{(l+1)} = V_{1_{j+1,k}}^{(l+1)} - \{\frac{\zeta_{j+1}}{\Delta\zeta}(\rho_{j+1,k}^{*(l)}U_{j+1,k}^{(l)} - \rho_{j,k}^*U_{j,k}) + 2\rho_{j+1,k}^{(l)}U_{j+1,k}^{(l)}\}\eta_k\Delta\eta \tag{62}$$

At the centerline $k = 0$, the continuity equation yields.

$$V_{1_{j+1,1}}^{(l+1)} = -\{\frac{\zeta_{j+1}}{\Delta\zeta}(\rho_{j+1,0}^{*(l)}U_{j+1,0}^{(l)} - \rho_{j,0}^{*}U_{j,0}) + 2\rho_{j+1,0}^{(l)}U_{j+1,0}^{(l)}\}\frac{(\Delta\eta)^2}{2} \tag{63}$$

The procedure of solution to the problem in this domain ($\eta - \zeta$ domain) is similar to that used in the previous section for the ($R - X$) coordinates.

The advantage of the second transformation is that in the first transformation increasing the number of grid points due to jet growth is necessary. In the second transformation, the number of grid points remains constant. Moving downstream, the radial step size (ΔR) effectively increases since $\Delta R = \Delta\eta\zeta$.

There is a problem with the second transformation whereby it cannot be started at $X = 0$ since η is infinite at this position. To solve this problem, the initial conditions for this transformation are taken at some location after the nozzle. The problem was solved in the ($R - X$) coordinates for the first few steps. The solutions obtained are used as initial conditions to the solution of the problem in the second transformation.

4. Results and Discussion

The results obtained are shown in Fig. 4-29. The first set of results begins with Fig. 4 and ends with Fig. 15. These figures show the velocity and mixture fraction profiles for all the considered gases at different normalized axial differences. Figures 4-7 are for $CO = 0.0$, Fig. 8-11 are for $CO = 0.5$ and Fig. 12-15 are for $CO = 0.75$. The mixture fraction profiles for the hydrogen jet aren't included because these values were too low that it was very difficult to show them on the same figure. This can be explained by noting that the hydrogen has the highest diffusion coefficient (lowest Sc number) and the lowest density (highest RMC) among the four considered jets. These two reasons give a high rate of decay for both the velocity and concentration of the hydrogen jet.

The second set of results aims to show the effect of changing the jet type on both the centerline velocity and mixture fraction. This effect has been shown for all values of CO considered. This set begins with Fig. 16 and ends with Fig. 21.

The last set of results aims to show the effect of changing the velocity ratio between the surrounding and the jet (CO) on both the centerline velocity and mixture fraction. This effect has been shown for all the jets considered. This set begins with Fig. 22 and ends with Fig. 29.

Inspection of the first set of results yields the following observations:

1. For $CO = 0.5$ and 0.75, there are dips in the velocity profiles close to the nozzle. Moving downstream, these dips disappear. This is due to interference between the jet and the moving surrounding. When the jet emerges from the nozzle, the particles of fluid that are close to the wall of the nozzle move at a very low velocity relative to the surrounding. When these particles mix with the moving surrounding, they retard it. Further downstream, these particles will continue to be accelerated by the surrounding until these dips disappear. This is consistent with the note that these dips don't appear when the surrounding is stagnant. These dips become deeper as the velocity of the surrounding increases.
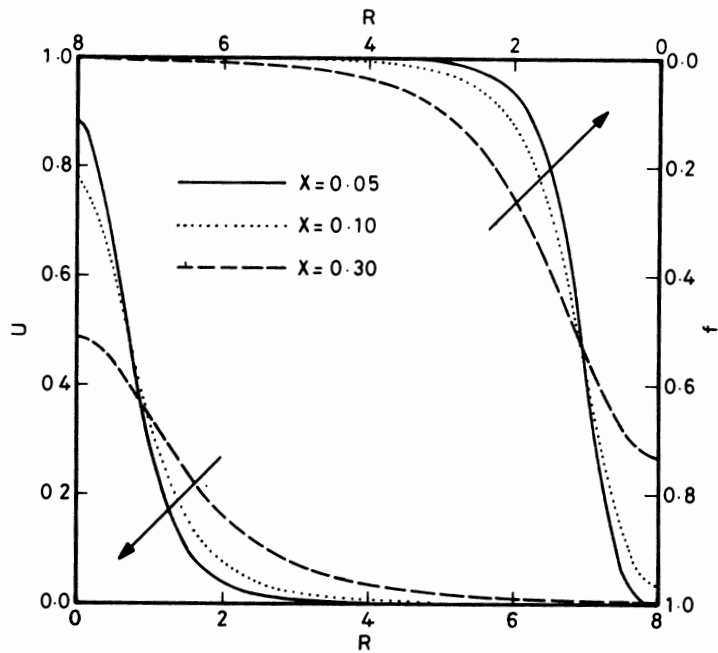
FIG. 4. Non-dimensional axial velocity and mixture fraction profiles at $CO = 0.0$ for the laminar CO_2 air jet.
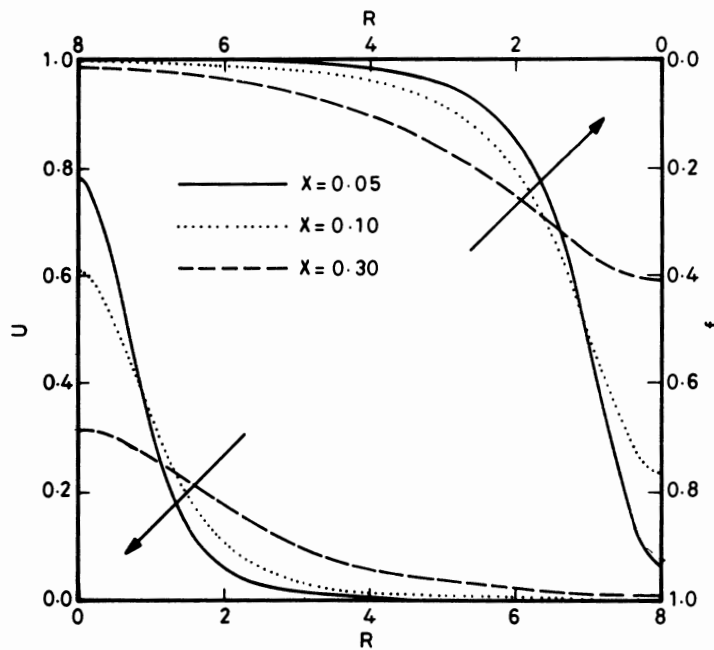

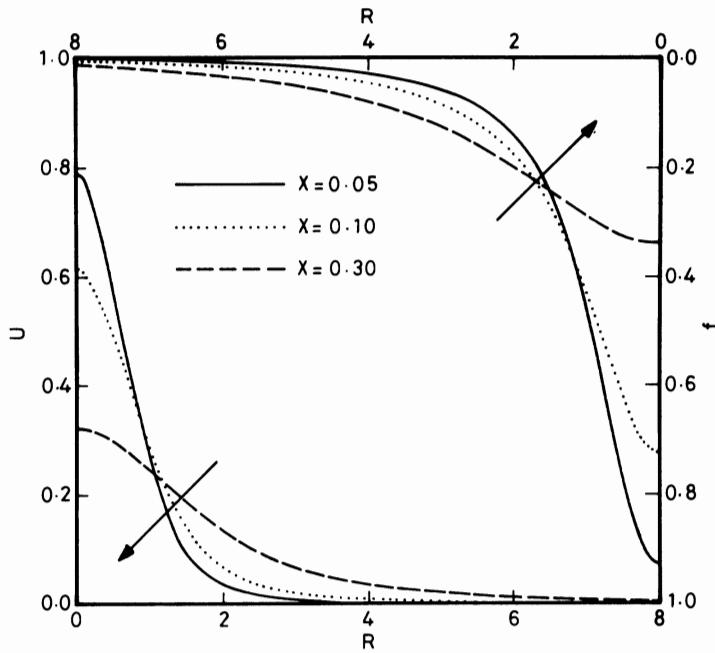FIG. 5. Non-dimensional axial velocity and mixture fraction profiles at $CO = 0.0$ for the laminar O_2 air jet.

FIG. 6. Non-dimensional axial velocity and mixture fraction profiles at $CO = 0.0$ for the laminar NH_3 air jet.
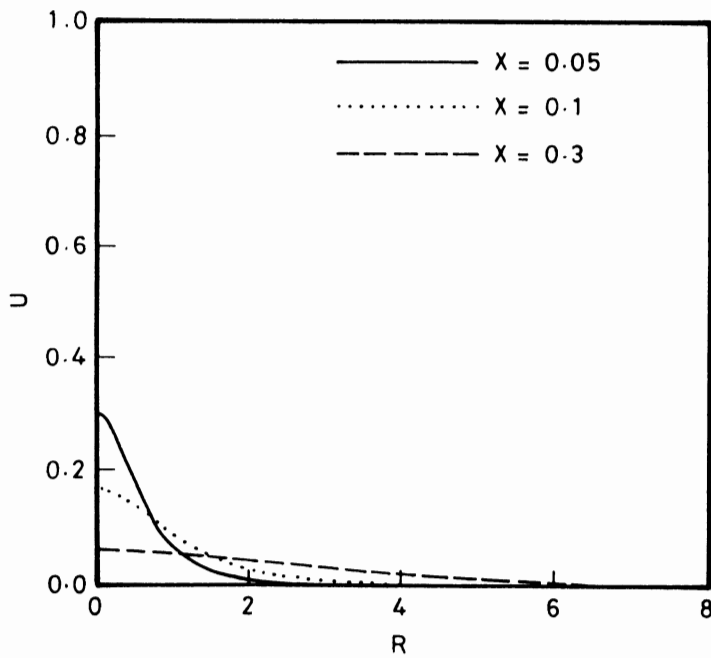

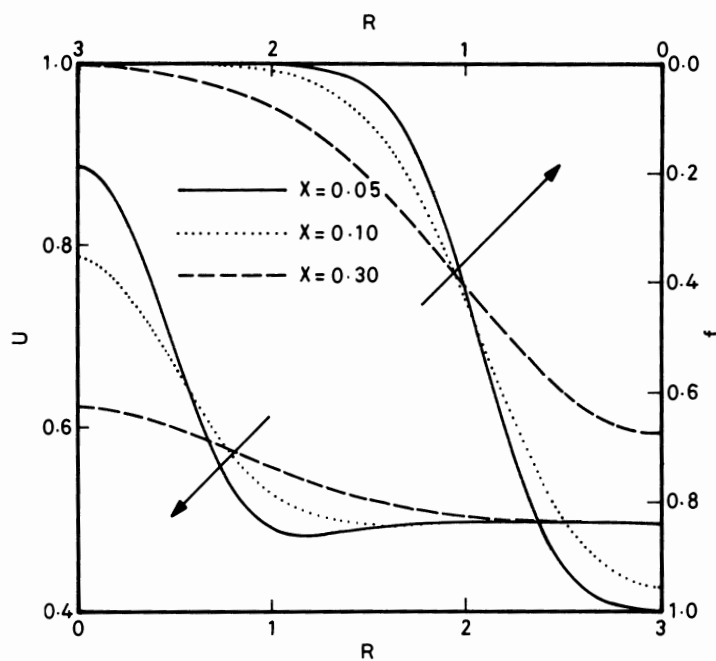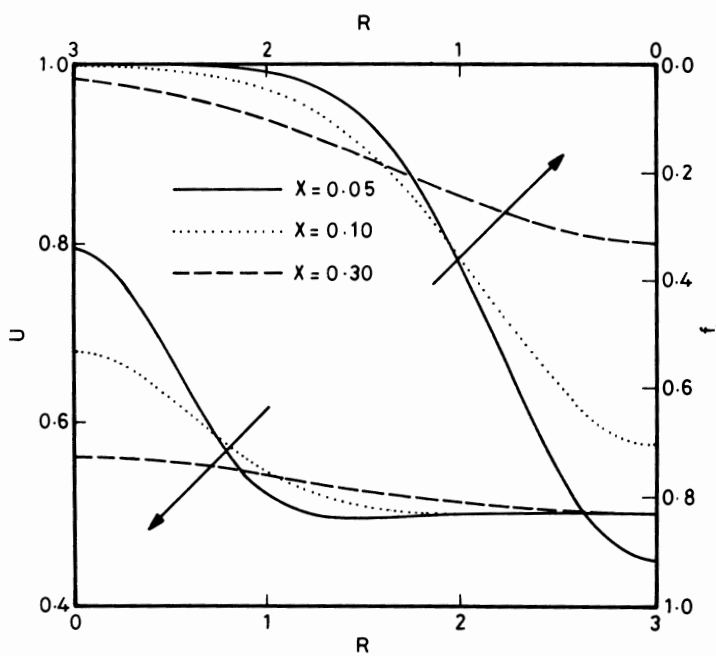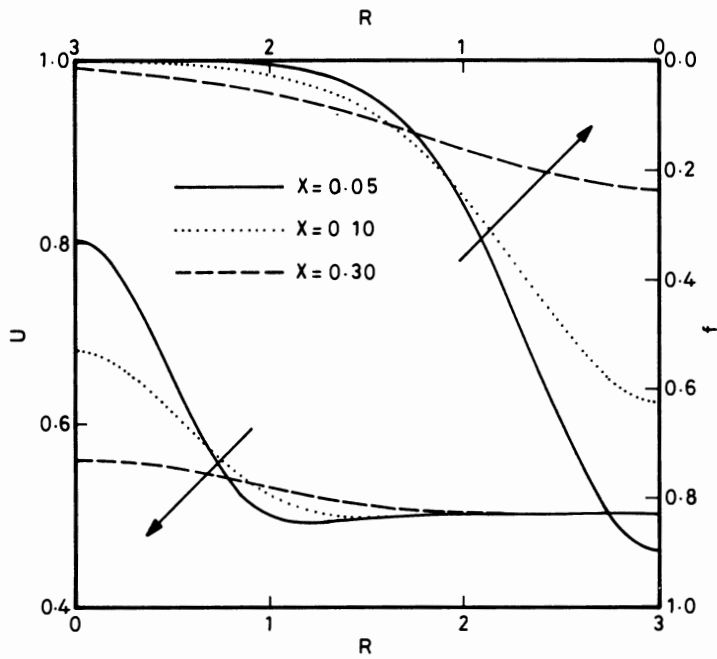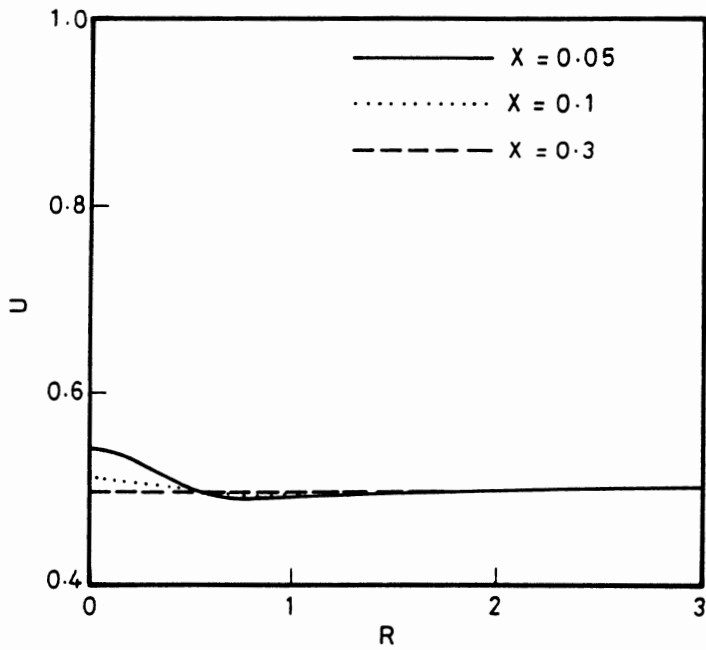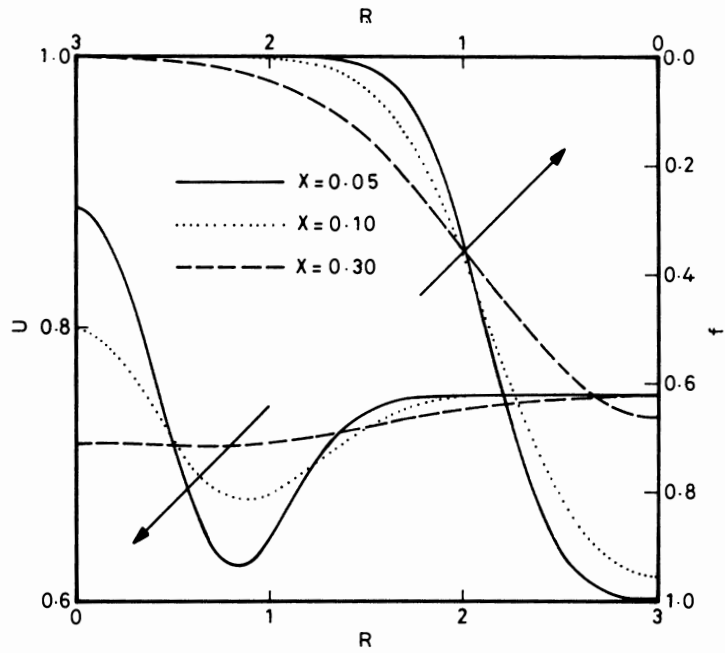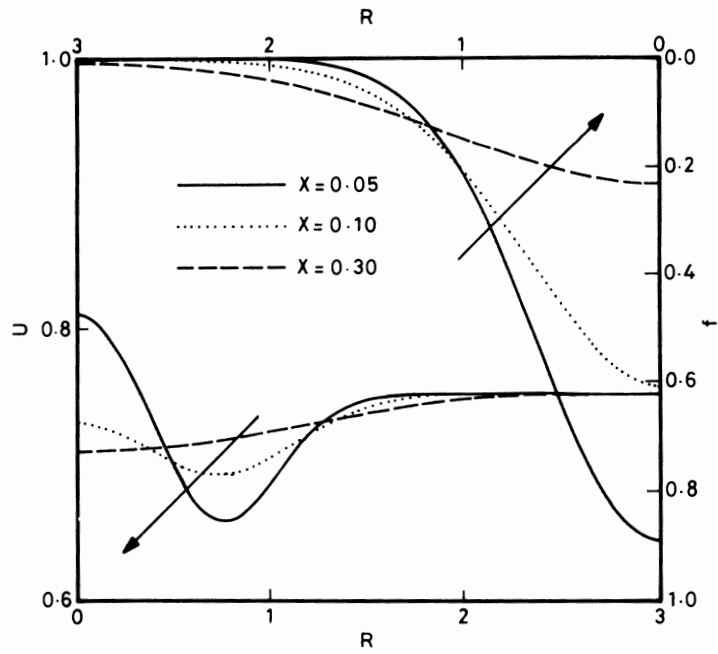FIG. 7. Non-dimensional axial velocity profiles at $CO = 0.0$ for the laminar H_2 air jet.

FIG. 8. Non-dimensional axial velocity and mixture fraction profiles at $CO = 0.5$ for the laminar CO_2 air jet.

FIG. 9. Non-dimensional axial velocity and mixture fraction profiles at $CO = 0.5$ for the laminar O_2 air jet.
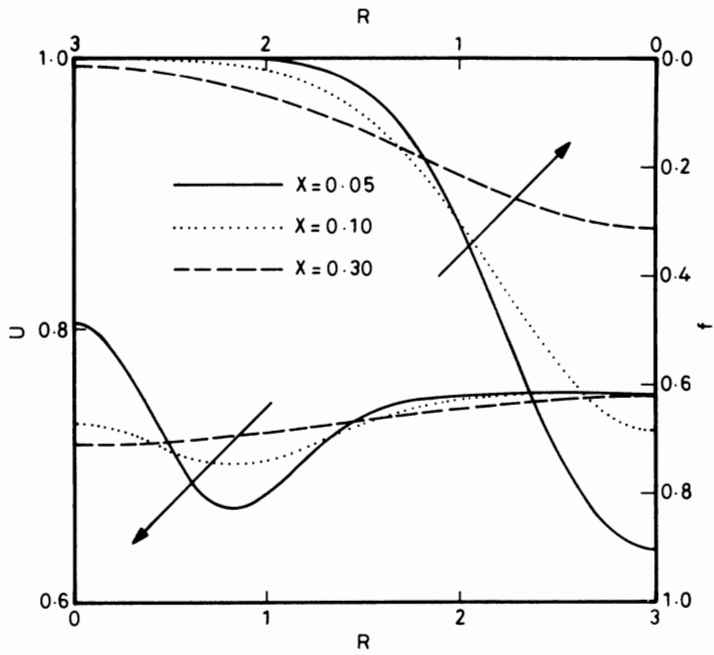
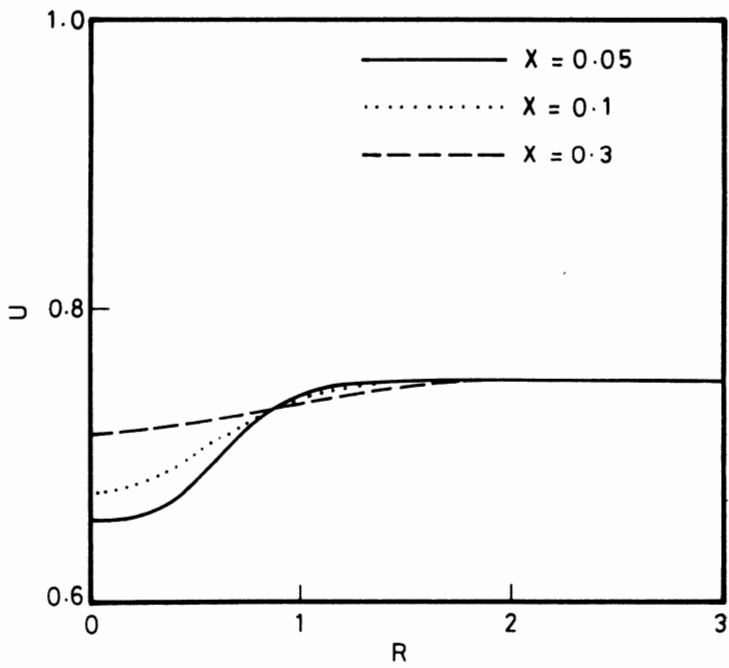FIG. 10. Non-dimensional axial velocity and mixture fraction profiles at $CO = 0.5$ for the laminar NH_3 air jet.

FIG. 11. Non-dimensional axial velocity profiles at $CO = 0.5$ for the laminar H_2 air jet.

FIG.12. Non-dimensional axial velocity and mixture fraction profiles at $CO = 0.75$ for the laminar CO_2 air jet.

FIG. 13. Non-dimensional axial velocity and mixture fraction profiles at $CO = 0.75$ for the laminar O_2 air jet.

FIG. 14. Non-dimensional axial velocity and mixture fraction profiles at $CO = 0.75$ for the laminar NH_3 air jet.
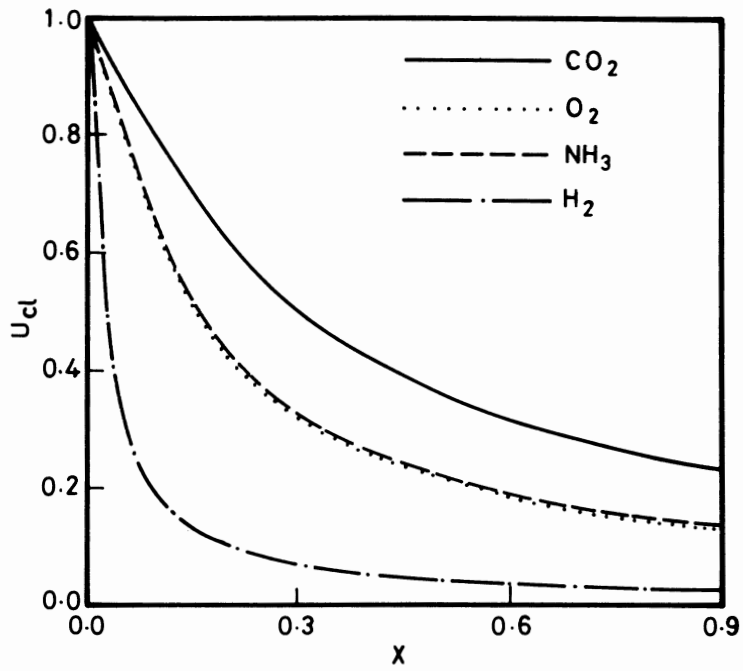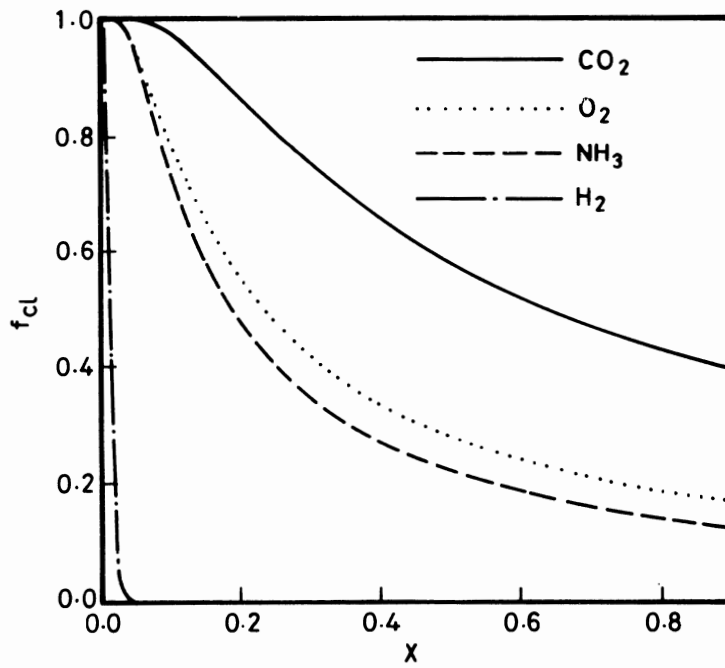

FIG. 15. Non-dimensional axial velocity profiles at $CO = 0.75$ for the laminar H_2 air jet.

FIG. 16. Decay of centerline velocity for CO_2, O_2, NH_3 and H_2 jets at $CO = 0.0$.

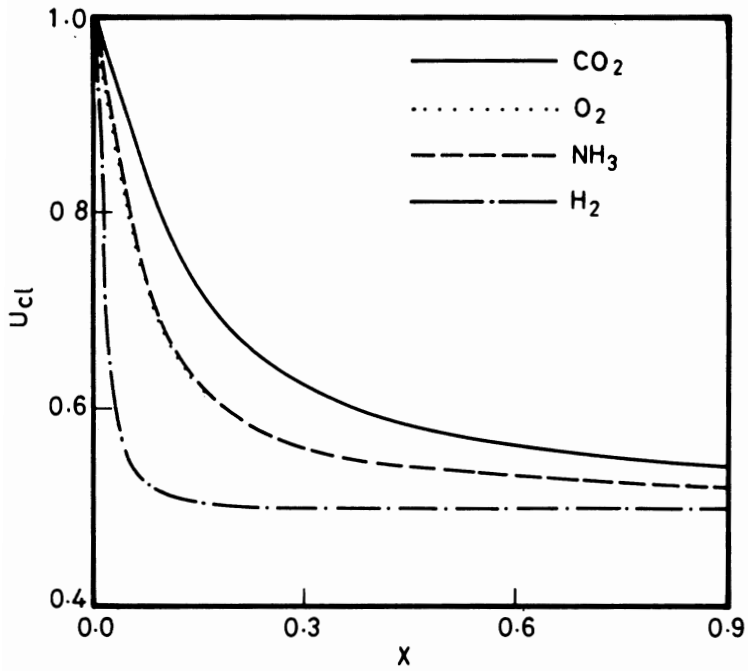FIG. 17. Decay of centerline mixture fraction for CO_2, O_2, NH_3 and H_2 jets at $CO = 0.0$.

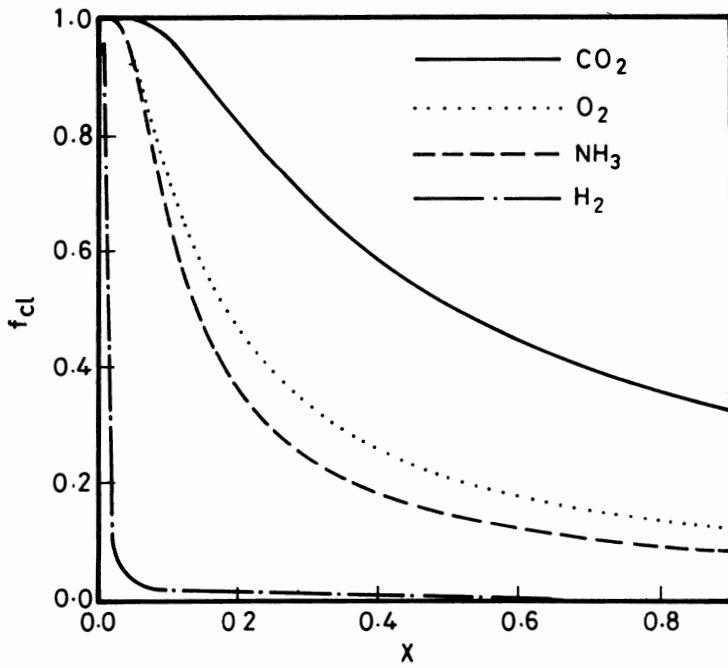FIG. 18. Decay of centerline velocity for CO_2, O_2, NH_3 and H_2 jets at $CO = 0.5$.

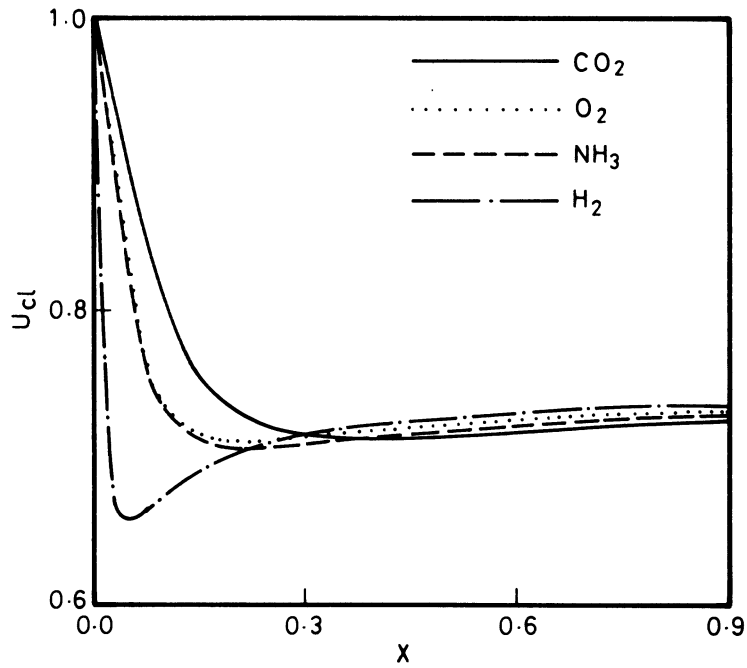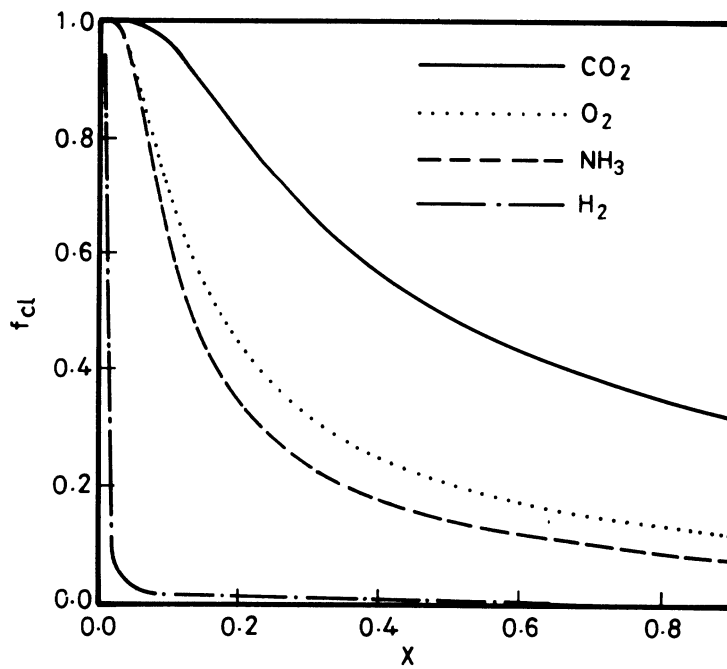FIG. 19. Decay of centerline mixture fraction for CO_2, O_2, NH_3 and H_2 jets at $CO = 0.5$.

Fig. 20. Decay of centerline velocity for CO_2, O_2, NH_3 and H_2 jets at $CO = 0.75$.

Fig. 21. Decay of centerline mixture fraction for CO_2, O_2, NH_3 and H_2 jets at $CO = 0.75$.

FIG. 22. Decay of the centerline velocity for the CO_2 air jet.

FIG. 23. Decay of the centerline mixture fraction for the CO_2 air jet.

FIG. 24. Decay of the centerline velocity for the O_2 air jet.

FIG. 25. Decay of the centerline mixture fraction for the O_2 air jet.

FIG. 26. Decay of the centerline velocity for the NH_3 air jet.

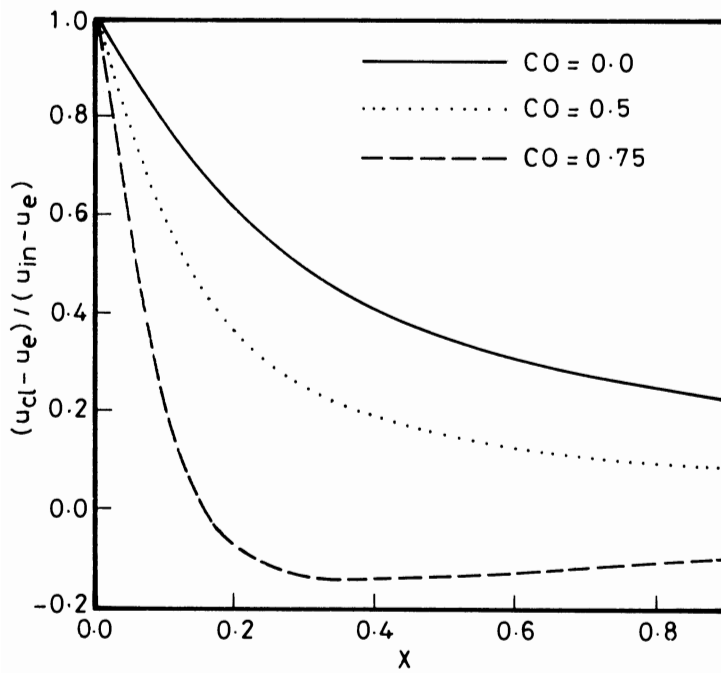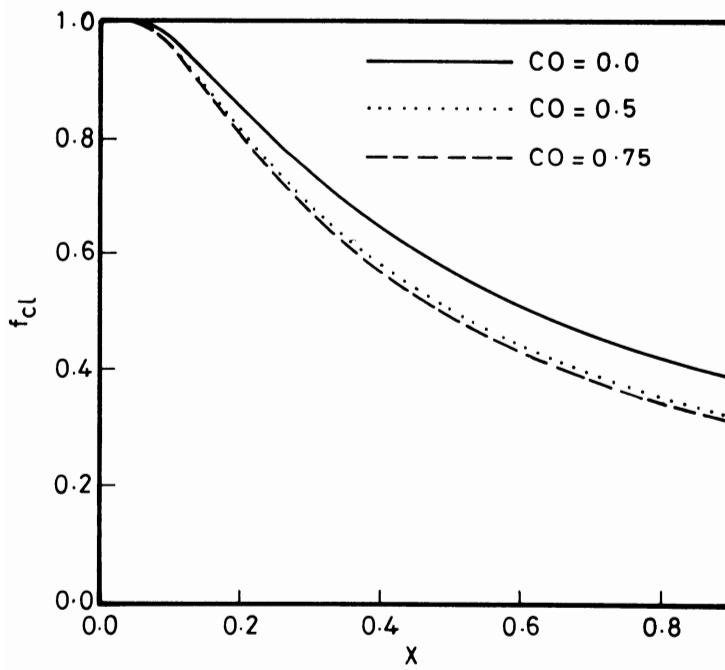FIG. 27. Decay of the centerline mixture fraction for the NH_3 air jet.
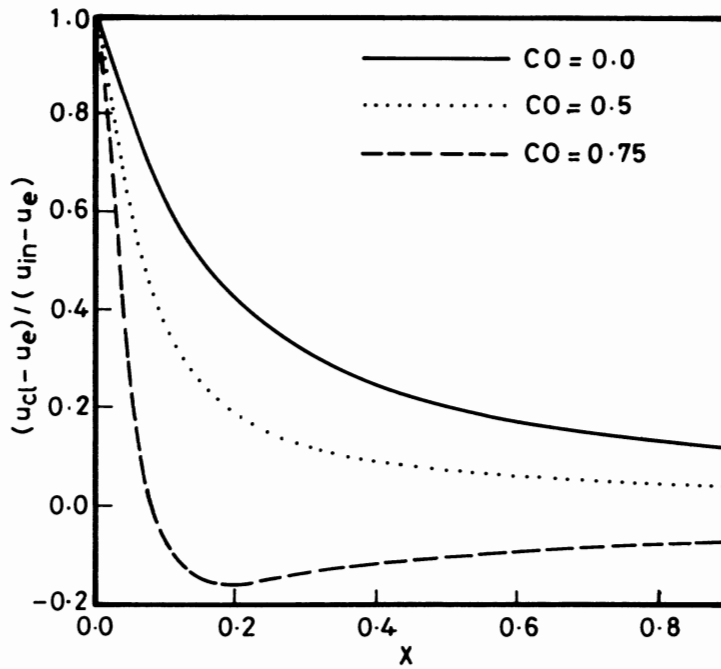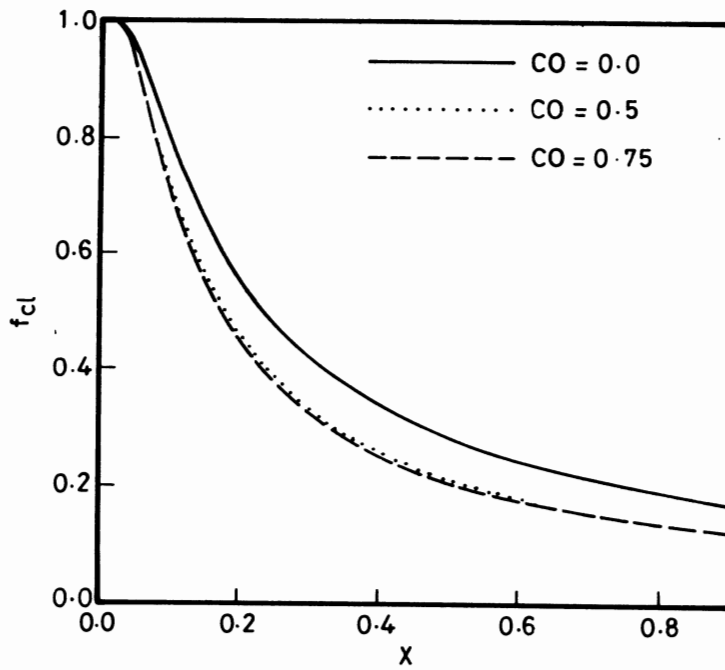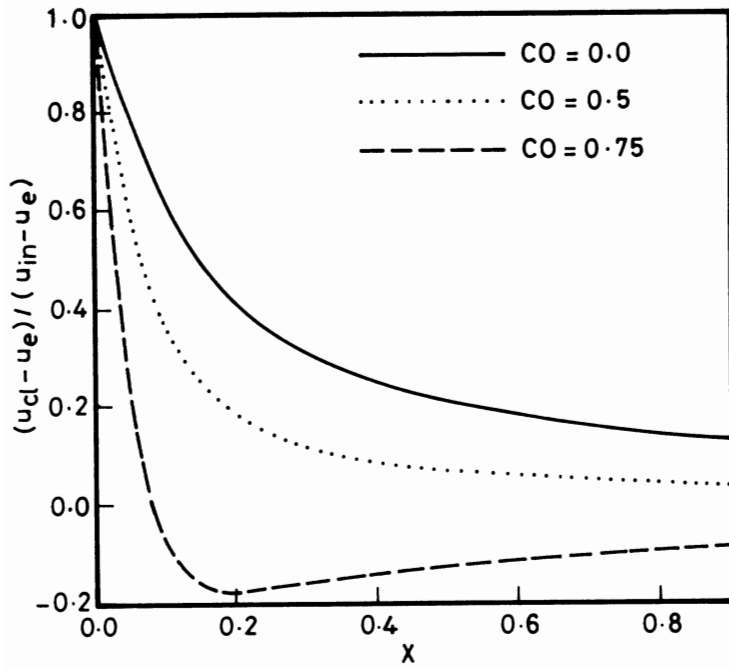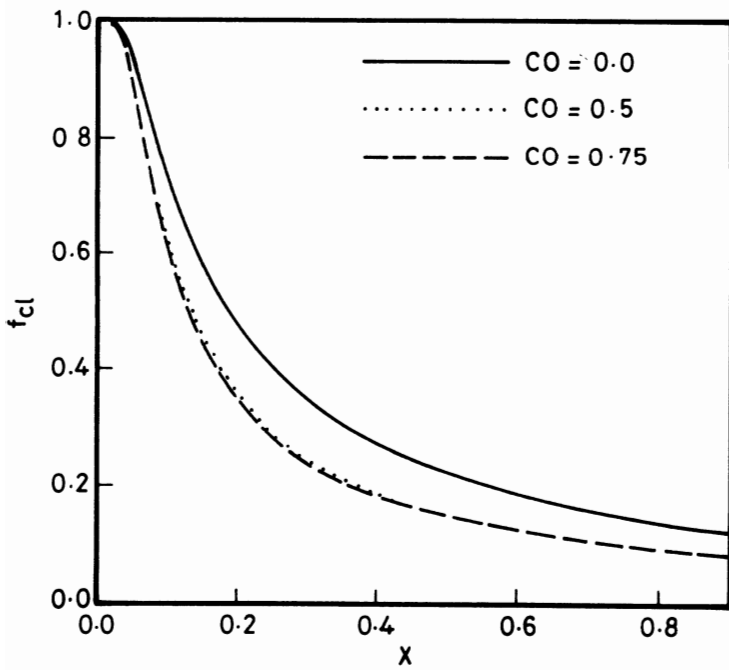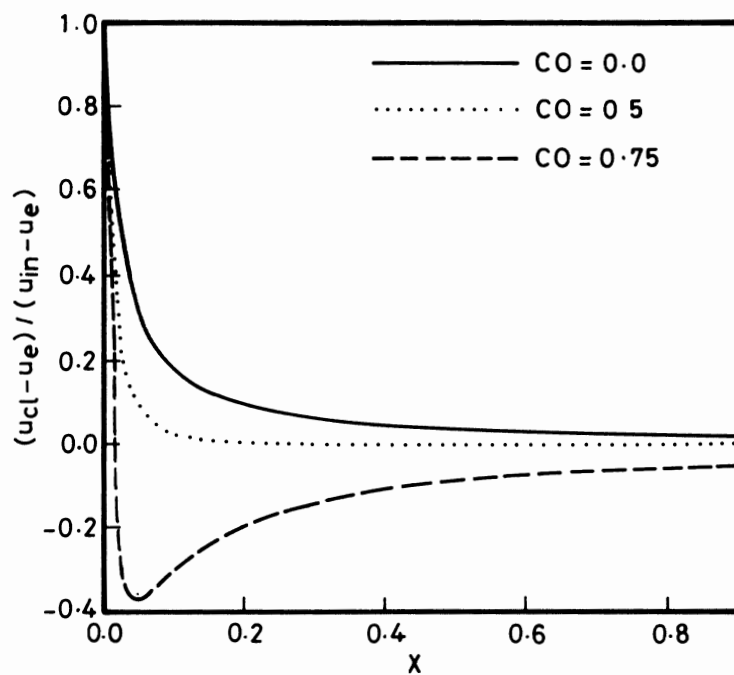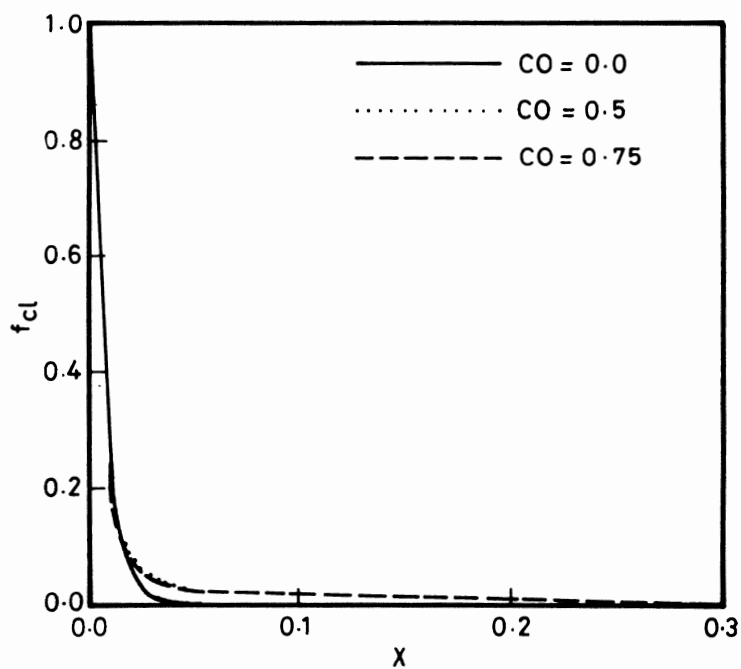
FIG. 28. Decay of the centerline velocity for the H_2 air jet.

FIG. 29. Decay of the centerline mixture fraction for the H_2 air jet.

2. When the surrounding is stagnant, the jet spreads very fast. As the surrounding moves, it gives a resistance to the spreading of the jet and thus limits its width. This can be seen by noting that at $CO = 0.0$, the jet width is approximately three times the jet width of $CO = 0.5$.

3. Comparison of the velocity and mixture fraction profiles for each gas considered shows that mass diffuses faster than momentum, because at any axial distance, the diffusion boundary layer is thicker than the momentum boundary layer. This can be explained by noting that $Sc = v/D$ where v is the kinematic viscosity and D is the diffusion coefficient. Since Sc number for all the studied jets is less than unity, hence the diffusion of momentum is slower than the diffusion of mass.

A look into the second set of results shows the following points:

1. The jets are classified according to the rate of decay of their centerline velocities in a descending manner as follows: Hydrogen, oxygen, ammonia and carbon dioxide. Oxygen and ammonia have approximately the same rate of decay. This can be explained on the basis of the ratio between the kinematic viscosity of the jet and that of the surrounding. When this ratio is small, then momentum will diffuse slowly and hence the jet will move a large distance before its velocity decays completely. A large value of the aforementioned ratio causes the momentum to diffuse rapidly so that the jet velocity decays with a relatively high rate. This ratio can be calculated for all the considered jets by multiplying μ^* by RMC for each jet. These values are given in Table 1. The results are shown in Table 2.

TABLE 2. Value of v_j/v_s for each jet.

jet	CO_2	O_2	NH_3	H_2
v_j/v_s^*	0.531	1.005	0.943	6.998

This behavior is independent of the surrounding velocity.

2. The jets are classified according to the rate of decay of their centerline mixture fraction in a descending manner as follows: Hydrogen, oxygen, ammonia and carbon dioxide. The explanation of this is somewhat different from that used for the centerline velocity. In this case, the controlling parameter is Π. A small value of Π means a slowly-diffusing gas, while a large one means a rapidly diffusing gas. This parameter will act in the same way mentioned in the previous point. Table 3 shows the value of Π for all the considered jets. This behaviour is independent of the value of the surrounding velocity.

TABLE 3. Value of Π for each jet.

jet	CO_2	O_2	NH_3	H_2
Π	0.564	1.34	1.208	31.811

3. It is noted that a dip in the centerline velocity becomes very apparent when $CO = 0.75$. This dip doesn't appear when $CO = 0.0$ and it has a low depth when $CO = 0.5$. This can be explained on the basis of the high sensitivity of the flow to

---

*Note that v_j/v_s for NH_3 and O_2 jets is approximately the same which explains the obtained result of the same rate of decay.

the selection of conditions at the nozzle exit. This explanation is supported by the result obtained after the same computer code had been run to the case when the initial velocity profile is uniform (*i.e.*, $U = 1.0$ at $R \leq 1$.). The result was that all the dips that appeared in the velocity profiles before disappeared. This can be seen from consideration of the momentum equation (7). Applying this equation at the centerline and using L'Hopital's rule give.

$$\rho_{cl}^* U_{cl} \frac{\partial U_{cl}}{\partial X} = 2\mu^* \frac{\partial^2 U_{cl}}{\partial R^2} |_{R=0.0} \tag{64}$$

The right hand side of this equation represents the momentum dissipation of the centerline velocity resulting from the shear stress. When the initial velocity profile is parabolic, then $\frac{\partial^2 U}{\partial R^2} |_{R=0.0}$ has a finite value which is relatively large while when the initial profile is uniform, this value is equal to zero. Based on this result, it can be concluded that $\frac{\partial U_{cl}}{\partial X}$ for the parabolic profile is higher than that for the uniform one. This means that in the region close to the nozzle, the centerline velocity decays faster when the initial profile is parabolic. The centerline velocity cannot continue decaying forever because finally, the jet has to move with the surrounding as one unit. So, after it had reached its absolute minimum, the centerline velocity increases until it reaches the surrounding velocity. As the surrounding velocity increases, this dip becomes deeper to cope with the high momentum dissipation rate caused by the parabolic initial condition.

Investigation of the last set of results reveals the following observations

1. Increase of surrounding velocity tends to enhance the decay of the centerline velocity and mixture fraction. The effect of the surrounding velocity on the centerline velocity is very clear and this effect increases as it increase. The effect on the centerline mixture fraction seems to be less apparent as the surrounding velocity increases beyond half the initial centerline velocity of the jet.

2. Remark 3 mentioned for the second set of results appears here again. It can be explained based on the same argument made there.

3. It is noted that the dip in the hydrogen centerline velocity is the deepest. This can be explained using Equation (64) where it implies that low density causes a high $\partial U_{cl}/\partial X$. Since the hydrogen has the lowest density (highest *RMC*) among the considered jets, then this magnified dip can be expected.

5. Conclusion

In this work, a numerical study is conducted for laminar jets. An implicit finite difference method is used to solve the boundary-layer equations governing the jet flow. A coordinate transformation is used to improve the efficiency and accuracy of the numerical scheme.

The computations are obtained for carbon dioxide, oxygen, ammonia and hydrogen jets issuing into air at the same temperature. The results are obtained for stagnant and co-flowing surroundings. The major conclusions are:

1. The flow is very sensitive to the initial conditions used for the solution, so one should be very careful when specifying these conditions.

2. Changing the jet gas can sometimes have a large effect on the decay of the jet. This depends on the ratio between the kinematic viscosity of the jet and that of the surrounding and also on the Sc number.

3. Increasing the surrounding velocity reduces the rate of growth of the jet and therefore reduces its rate of decay.

References

[1] **Hijazen, B.B.** and **Rabadi, N.J.,** Computations of axisymmetric non-reacting Jets, *International Journal of Heat and Technology.* **11**(1-2) (1993).

[2] **Hijazen, B.B.,** *Computations of Axisymmetric Non-Reacting and Reacting Jets.* MS Thesis, University of Illinois at Chicago, USA (1989).

[3] **Ghazzawi, N.A.,** *Computations of Axisymmetric Turbulent and Laminar Non-Reacting Jets Issuing into a Moving Medium.* M.S. Thesis, University of Jordan, Amman, Jordan (1992).

[4] **Hijazen, B.B.** and **Rabadi, N.J.,** Computations of Axisymmetric Turbulent Non-Reacting Jets, University of Jordan, *Dirasat,* **20B**(3): 131-147 (1993).

[5] **Anderson, D.A., Tannehill, J.C.** and **Pleteher, R.H.,** *Computational Fluid Mechanics and Heat Transfer.* Hemisphere, New York (1984).

[6] **Pai, Shih-I.,** *Fluid Dynamics of Jets.* D. Van Nostrand Co., Inc. (1954).

[7] **Rohensow, W.M.** and **Choi, H.Y.,** *Heat, Mass, and Momentum Transfer,* Prentice-Hall, Inc. (1961).

[8] **Bird, R.B., Stewart, W.E.** and **Lightfoot, E.N.,** *Transport Phenomena,* John Wiley & Sons, Inc. (1960).

[9] **Hornbeck, R.W.,** *Numerical Marching Techniques for Fluid Flow with Heat Transfer,* NASA SP-297, Washington, D.C. (1973).

[10] **Holman, J.P.,** *Heat Transfer,* McGraw-Hill Book Company (1989).

[11] **Kee, R.J.** and **Miller, J.A.,** *A Split-Operator Finite Difference Solution for Axisymmetric Laminar Jet Diffusion Flames,* Sandia Laboratories, Rept. SAND77-8502, Albuquerque, New Mexico (1977).

Nomenclature

a	initial radius of the jet (m);
A_1, B_1, C_1, D_1	coefficients (Equation (44));
A_2, B_2, C_2, D_2	coefficients (Equation (53));
CO	co-flowing parameter, $CO = u_e/u_{in}$;
d	diameter of the exit nozzle, $d = 2a$ (m);
D	diffusion coefficient;
f	ratio of the weight of the injected gas to that of the mixture;
r	radial distance (m);
R	dimensionless radial distance r. $(R = r/a)$;
Re	Reynolds number;
RMC	ratio of the ambient density to the jet density;
Sc	Schmidt number, $Sc = \mu/\rho D_j$;
u	axial velocity (m/sec);
U	normalized u;
υ	lateral velocity (m/sec);
V	normalized υ;
x	axial coordinate (m);
X	normalized x (m);

Greek Symbols

$\alpha, \beta, \omega, \Phi$	coefficients (Equation (14));
$\alpha', \beta', \omega', \Phi'$	coefficients (Equation (25));

ΔR	nondimensional step size in the radial direction;
ΔX	nondimensional step size in the axial direction;
η	transformed radial coordinate in the second transformation;
$\Delta\eta$	nondimensional step size in the η direction;
μ	viscosity (N. sec/m^2);
v	laminar kinematic viscosity (m^2/sec);
Π	parameter $= \mu* RMC/Sc;$
ρ	density (kg/m$^{3)}$;
ζ	transformed axial coordinate in the second transformation;

Subscripts

in	initial centerline value;
j	axial node index;
k	radial node index;
0	reference quantity;
∞	ambient air;
e	jet edge;

Superscripts

| * | normalized quantity |

حـل عـددي للنـفث المتماثـل الطبـقي القـابل للانضغـاط في الأوسـاط المتحركة وغـير المتحركة

نضال غزاوي ، و نصري الربضي ، و باسم حجازين

قسم الهندسة الميكانيكية ، كلية الهندسة والتكنولوجيا ، الجامعة الأردنية

عمـــــان – الأردن

المستخلص .   أجريت دراسة عددية لفهم النفث الطبقي القابل للانضغاط ، حيث اعتبر الوسط الذي ينبعث فيه النفث هواءً ساكنًا أو متحركًا في نفس اتجاه حركة النفث . وقد أجريت الدراسة لأربعة أنواع من الغازات المستخدمة في النفث ، وهي ثاني أكسيد الكربون ، والأكسجين ، والأمونيا ، والهيدروجين .

استُخدمت طريقة الفرق المحدود الضمنية في حل معادلات الطبقة المتاخمة للنفث ، حيث استخدم تحويل خاص لمحاور النفث لتحسين كفاءة الحل العددي . وقد تم عرض النتائج لتغير السرعات ونسبة المزج بين غاز النفث والهواء ، كما أجريت دراسة مقارنة لهذه النتائج للغازات الأربعة .